


 Cite this: *RSC Adv.*, 2022, **12**, 24260

Effects of coordinating heteroatoms on molecular structure, thermodynamic stability and redox behavior of uranyl(vi) complexes with pentadentate Schiff-base ligands†

Tomoyuki Takeyama * and Koichiro Takao *

Uranyl(vi) complexes with pentadentate N_3O_2^- , N_2O_3^- and $\text{N}_2\text{O}_2\text{S}_1^-$ -donating Schiff base ligands, $\text{tBu}_3\text{MeO}-\text{saldien}-\text{X}^{2-}$ ($\text{X} = \text{NH}$, O and S), were synthesized and thoroughly characterized by ^1H NMR, IR, elemental analysis, and single crystal X-ray diffraction. The crystal structures of $\text{UO}_2(\text{tBu}_3\text{MeO}-\text{saldien}-\text{X})$ showed that the $\text{U}-\text{X}$ bond strength follows $\text{U}-\text{O} \approx \text{U}-\text{NH} > \text{U}-\text{S}$. Conditional stability constants (β_{X}) of $\text{UO}_2(\text{tBu}_3\text{MeO}-\text{saldien}-\text{X})$ in ethanol were investigated to understand the effect of X on thermodynamic stability. The $\log \beta_{\text{X}}$ decrease in the order of $\text{UO}_2(\text{tBu}_3\text{MeO}-\text{saldien}-\text{NH})$ ($\log \beta_{\text{NH}} = 10$) $> \text{UO}_2(\text{tBu}_3\text{MeO}-\text{saldien}-\text{O})$ ($\log \beta_{\text{O}} = 7.24$) $> \text{UO}_2(\text{tBu}_3\text{MeO}-\text{saldien}-\text{S})$ ($\log \beta_{\text{S}} = 5.2$). This trend cannot be explained only by Pearson's Hard and Soft Acids and Bases (HSAB) principle, but rather follows the order of basicity of X . Theoretical calculations of $\text{UO}_2(\text{tBu}_3\text{MeO}-\text{saldien}-\text{X})$ suggested that the ionic character of $\text{U}-\text{X}$ bonds decreases in the order of $\text{U}-\text{NH} > \text{U}-\text{O} > \text{U}-\text{S}$, while the covalency increases in the order $\text{U}-\text{O} < \text{U}-\text{NH} < \text{U}-\text{S}$. Redox potentials of all $\text{UO}_2(\text{tBu}_3\text{MeO}-\text{saldien}-\text{X})$ in DMSO were similar to each other regardless of the difference in X . Spectroelectrochemical measurements and DFT calculations revealed that the center U^{6+} of each $\text{UO}_2(\text{tBu}_3\text{MeO}-\text{saldien}-\text{X})$ undergoes one-electron reduction to afford the corresponding uranyl(v) complex. Consequently, the difference in X of $\text{UO}_2(\text{tBu}_3\text{MeO}-\text{saldien}-\text{X})$ affects the coordination of $\text{tBu}_3\text{MeO}-\text{saldien}-\text{X}^{2-}$ with UO_2^{2+} . However, the HSAB principle is not always prominent, but the Lewis basicity and balance between ionic and covalent characters of the $\text{U}-\text{X}$ interactions are more relevant to determine the bond strengths.

 Received 25th July 2022
 Accepted 22nd August 2022

 DOI: 10.1039/d2ra04639c
rsc.li/rsc-advances

Introduction

Uranium is the most important element in nuclear engineering. The chemistry of uranium plays important roles in nuclear fuel fabrication and spent fuel reprocessing. Under ambient conditions, uranium is most commonly present as a hexavalent uranyl(vi) ion, UO_2^{2+} , with a typical linear $[\text{O} \equiv \text{U}^{\text{VI}} \equiv \text{O}]^{2+}$ structure. The chemical separation of UO_2^{2+} from various aqueous systems such as feed solutions of spent nuclear fuels and even seawater is one of the important research topics in nuclear chemistry. In the usual sense, coordination chemistry provides very powerful tools for chemical separation. Hence, the

complexation between UO_2^{2+} and organic ligands has been widely studied.^{1–13}

Pearson's Hard and Soft Acids and Bases (HSAB) principle is quite useful to describe preferential interactions between specific metal ions and coordinating atoms of ligands and to design organic molecules selectively coordinating with a target metal ion,^{14,15} although this principle is rather empirical. In the HSAB principle, UO_2^{2+} is classified as a hard acid,^{14,15} and therefore, generally tends to more strongly interact with hard bases like N , O and F , compared with softer ones such as heavier congeners like P , S , and Cl .^{14,15} Indeed, thermodynamic stability of a UO_2^{2+} -halido complex in DMF follows the order of hardness of halide ligands, $\text{Cl}^- > \text{Br}^- > \text{I}^-$.¹⁶ In contrast, such a trend in complexation between UO_2^{2+} and heteroatoms like N , O and S , seems not to be well understood systematically, although it would provide essential information to understand the fundamental nature of UO_2^{2+} in more depth and to design molecular structures of ligands exclusively interacting with UO_2^{2+} . Indeed, several extracting reagents have been successfully developed for separation of $\text{Am}(\text{m})$ and $\text{Cm}(\text{m})$ from $\text{Ln}(\text{m})$ on the basis of difference in coordinating affinities of these metal ions with soft-donor atoms incorporated in the designed ligands.^{17–20}

Laboratory for Zero-Carbon Energy, Institute of Innovative Research, Tokyo Institute of Technology, 2-12-1 N1-32, O-Okayama, Meguro-ku, Tokyo 152-8550, Japan. E-mail: takeyama.t.ab@m.titech.ac.jp; takao.k.ac@m.titech.ac.jp

† Electronic supplementary information (ESI) available: Crystallographic data of $\text{UO}_2(\text{L}_\text{X})$, crystal structure of $\text{H}_2\text{L}_\text{S}$, electrochemical data, spectroelectrochemical data, and optimized structures and structural parameters of $[\text{UO}_2(\text{L}_\text{X})]^{10-}$. CCDC 2177295 for $\text{UO}_2(\text{L}_\text{O}) \cdot (\text{C}_5\text{H}_5\text{N})$, 2177296 for $\text{UO}_2(\text{L}_\text{S}) \cdot (\text{CH}_2\text{Cl}_2)$ and 2177297 for $\text{UO}_2(\text{L}_\text{NH}) \cdot (\text{CH}_2\text{Cl}_2)$. For ESI and crystallographic data in CIF or other electronic format see <https://doi.org/10.1039/d2ra04639c>



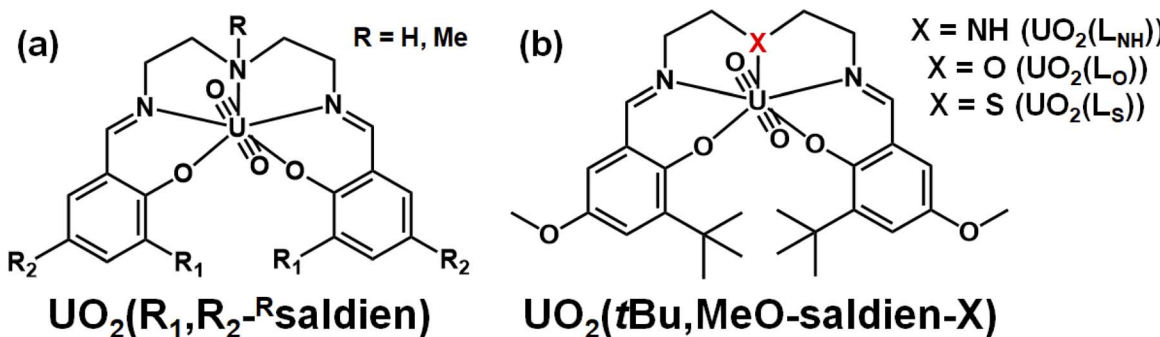


Fig. 1 Schematic structures of $\text{UO}_2(\text{R}_1, \text{R}_2, -\text{R}\text{-saldien})^{21,22}$ (a) and $\text{UO}_2(\text{tBu, MeO-saldien-X})$ complexes ($\text{UO}_2(\text{L}_X)$); ($\text{X} = \text{NH, O, S}$) (b).

In this study, we discuss strengths of U–N, U–O and U–S interactions formed in UO_2^{2+} complexes having analogous coordination geometries. For this purpose, it is first necessary to choose a suitable ligand system. Previously, we reported UO_2^{2+} complexes with N_3O_2 -pentadentate Schiff base ligands, $\text{UO}_2(\text{R}_1, \text{R}_2, -\text{R}\text{-saldien})$, shown in Fig. 1(a).^{21,22} Its NR moiety can be substituted with O or S to provide the similar UO_2^{2+} complexes, $\text{UO}_2(\text{tBu, MeO-saldien-X})$ ($\text{UO}_2(\text{L}_X)$, $\text{X} = \text{NH, O, S}$, Fig. 1(b)), where the U–O or U–S bond will be formed instead of U–NR. Here, we report synthesis and characterization of $\text{UO}_2(\text{L}_X)$ ($\text{X} = \text{NH, O, S}$) to discuss effects of X to the U–X bond strength and thermodynamic stability as well as redox chemistry of this class of UO_2^{2+} complexes.

Experimental section

Materials and syntheses

All reagents used were of reagent grade and used as received, if not specified. 3-*tert*-Butyl-5-methoxysalicylaldehyde was synthesized as reported elsewhere.²³

$\text{UO}_2(\text{tBu, MeO-Saldien-NH})$ ($\text{UO}_2(\text{L}_{\text{NH}})$). To a solution of 3-*tert*-butyl-5-methoxysalicylaldehyde (202 mg, 0.971 mmol) in ethanol (2 mL) was added 2,2'-diaminodiethylamine (52.1 μL , 0.480 mmol). This solution was heated to reflux for 10 min. $\text{UO}_2(\text{NO}_3)_3 \cdot 6\text{H}_2\text{O}$ (210 mg, 0.418 mmol) dissolved in ethanol (2 mL) was dropwise added to the solution. A red precipitate was formed within several minutes, and the suspension was stirred at 60 °C for 1 h. After cooling to room temperature, a red precipitate was collected by filtration and rinsed with methanol. Recrystallization from CH_2Cl_2 /ethanol yielded red crystals. Yield: 176 mg (48%). This compound was characterized by ^1H NMR, IR and elemental analysis. ^1H NMR (399.78 MHz, CD_2Cl_2 , δ/ppm vs. TMS): 1.71 (s, 18H, $-\text{C}(\text{CH}_3)_3$), 3.83 (s, 6H, $\text{O}-\text{CH}_3$), 4.59 (m, 4H, $\text{C}=\text{N}-\text{CH}_2\text{CH}_2-\text{O}$ or $\text{C}=\text{N}-\text{CH}_2\text{CH}_2-\text{O}$), 4.65 (m, 4H, $\text{C}=\text{N}-\text{CH}_2\text{CH}_2-\text{O}$ or $\text{C}=\text{N}-\text{CH}_2\text{CH}_2-\text{O}$), 6.91 (d, 2H, aryl, $J_{\text{H}-\text{H}} = 3.2$ Hz), 7.33 (d, 2H, aryl, $J_{\text{H}-\text{H}} = 3.6$ Hz), 9.50 (s, 2H, $\text{N}=\text{CH}-$). ^1H NMR (399.78 MHz, $\text{DMSO}-d_6$, δ/ppm vs. TMS): 1.64 (s, 18H, $-\text{C}(\text{CH}_3)_3$), 3.77 (s, 6H, $\text{O}-\text{CH}_3$), 4.53 (t, 4H, $\text{C}=\text{N}-\text{CH}_2\text{CH}_2-\text{O}$ or $\text{C}=\text{N}-\text{CH}_2\text{CH}_2-\text{O}$, $J_{\text{H}-\text{H}} = 5.2$ Hz), 4.66 (t, 4H, $\text{C}=\text{N}-\text{CH}_2\text{CH}_2-\text{O}$ or $\text{C}=\text{N}-\text{CH}_2\text{CH}_2-\text{O}$, $J_{\text{H}-\text{H}} = 5.2$ Hz), 7.09 (d, 2H, aryl, $J_{\text{H}-\text{H}} = 3.2$ Hz), 7.17 (d, 2H, aryl, $J_{\text{H}-\text{H}} = 3.6$ Hz), 9.75 (s, 2H, $\text{N}=\text{CH}-$). IR (ATR, cm^{-1}): 883 ($\text{O}=\text{U}=\text{O}$ asymmetric stretching, ν_3), 1637 ($\text{C}=\text{N}$ stretching, $\nu_{\text{C}=\text{N}}$). Elemental analysis (%) calcd for $\text{UO}_2(\text{L}_{\text{NH}})$ ($\text{C}_{28}\text{H}_{39}\text{N}_3\text{O}_6\text{U}_1$): C, 44.74; H, 5.23; N, 5.59. Found: C 44.64; H, 5.29; N, 5.42. The obtained crystals were also suitable for X-ray crystallography.

(ATR, cm^{-1}): 858 ($\text{O}=\text{U}=\text{O}$ asymmetric stretching, ν_3), 1636 ($\text{C}=\text{N}$ stretching, $\nu_{\text{C}=\text{N}}$). Elemental analysis (%) calcd for $\text{UO}_2(\text{L}_{\text{NH}})$ ($\text{C}_{28}\text{H}_{39}\text{N}_3\text{O}_6\text{U}_1$): C, 44.74; H, 5.23; N, 5.59. Found: C 44.64; H, 5.29; N, 5.42. The obtained crystals were also suitable for X-ray crystallography.

$\text{UO}_2(\text{tBu, MeO-Saldien-O})$ ($\text{UO}_2(\text{L}_{\text{O}})$). To a solution of 3-*tert*-butyl-5-methoxysalicylaldehyde (50.7 mg, 0.243 mmol) in ethanol (3 mL) was added 2,2'-oxybis(ethylamine) (12.6 μL , 0.119 mmol). This solution was heated to reflux for 10 min. $\text{UO}_2(\text{NO}_3)_3 \cdot 6\text{H}_2\text{O}$ (210 mg, 0.418 mmol) dissolved in ethanol (2 mL) was dropwise added to the solution. A red precipitate was formed within several minutes, and the suspension was stirred at 60 °C for 1 h. After cooling to room temperature, a red precipitate was collected by filtration and rinsed with methanol. Recrystallization from CH_2Cl_2 /ethanol yielded red microcrystals. Yield: 27.1 mg (30%). This compound was characterized by ^1H NMR, IR and elemental analysis. ^1H NMR (399.78 MHz, CD_2Cl_2 , δ/ppm vs. TMS): 1.71 (s, 18H, $-\text{C}(\text{CH}_3)_3$), 3.83 (s, 6H, $\text{O}-\text{CH}_3$), 4.59 (m, 4H, $\text{C}=\text{N}-\text{CH}_2\text{CH}_2-\text{O}$ or $\text{C}=\text{N}-\text{CH}_2\text{CH}_2-\text{O}$), 4.65 (m, 4H, $\text{C}=\text{N}-\text{CH}_2\text{CH}_2-\text{O}$ or $\text{C}=\text{N}-\text{CH}_2\text{CH}_2-\text{O}$), 6.91 (d, 2H, aryl, $J_{\text{H}-\text{H}} = 3.2$ Hz), 7.33 (d, 2H, aryl, $J_{\text{H}-\text{H}} = 3.6$ Hz), 9.50 (s, 2H, $\text{N}=\text{CH}-$). ^1H NMR (399.78 MHz, $\text{DMSO}-d_6$, δ/ppm vs. TMS): 1.64 (s, 18H, $-\text{C}(\text{CH}_3)_3$), 3.77 (s, 6H, $\text{O}-\text{CH}_3$), 4.53 (t, 4H, $\text{C}=\text{N}-\text{CH}_2\text{CH}_2-\text{O}$ or $\text{C}=\text{N}-\text{CH}_2\text{CH}_2-\text{O}$, $J_{\text{H}-\text{H}} = 5.2$ Hz), 4.66 (t, 4H, $\text{C}=\text{N}-\text{CH}_2\text{CH}_2-\text{O}$ or $\text{C}=\text{N}-\text{CH}_2\text{CH}_2-\text{O}$, $J_{\text{H}-\text{H}} = 5.2$ Hz), 7.09 (d, 2H, aryl, $J_{\text{H}-\text{H}} = 3.2$ Hz), 7.17 (d, 2H, aryl, $J_{\text{H}-\text{H}} = 3.6$ Hz), 9.75 (s, 2H, $\text{N}=\text{CH}-$). IR (ATR, cm^{-1}): 883 ($\text{O}=\text{U}=\text{O}$ asymmetric stretching, ν_3), 1637 ($\text{C}=\text{N}$ stretching, $\nu_{\text{C}=\text{N}}$). Elemental analysis (%) calcd for $\text{UO}_2(\text{L}_{\text{O}})$ ($\text{C}_{28}\text{H}_{38}\text{N}_2\text{O}_7\text{U}_1$): C, 44.68; H, 5.09; N, 3.72. Found: C 44.79; H, 5.21; N, 3.65. The crystals suitable for X-ray diffraction were obtained by recrystallization from pyridine/hexane.

$\text{UO}_2(\text{tBu, MeO-Saldien-S})$ ($\text{UO}_2(\text{L}_{\text{S}})$). To a solution of 3-*tert*-butyl-5-methoxysalicylaldehyde (54.4 mg, 0.261 mmol) in ethanol (3 mL) was added 2,2'-thiobis(ethylamine) (14.5 μL , 0.126 mmol). This solution was heated to reflux for 10 min under Ar. $\text{UO}_2(\text{NO}_3)_3 \cdot 6\text{H}_2\text{O}$ (210 mg, 0.418 mmol) dissolved in ethanol (2 mL) was dropwise added to the solution under Ar. A dark red precipitate was formed within several minutes, and the suspension was stirred at 60 °C for 1 h. After cooling to room temperature, a red precipitate was collected by filtration quickly, and rinsed with deoxygenated ethanol. Recrystallization from CH_2Cl_2 /ethanol yielded dark red plate crystals. Yield: 7.8 mg (8%). This compound was characterized by ^1H NMR, IR



and elemental analysis. ^1H NMR (399.78 MHz, CD_2Cl_2 , δ /ppm vs. TMS): 1.70 (s, 18H, $-\text{C}(\text{CH}_3)_3$), 3.74 (br, 4H, $\text{C}=\text{N}-\text{CH}_2\text{CH}_2-\text{S}$ or $\text{C}=\text{N}-\text{CH}_2\text{CH}_2-\text{S}$), 3.83 (s, 6H, $\text{O}-\text{CH}_3$), 3.74 (s, 4H, $\text{C}=\text{N}-\text{CH}_2\text{CH}_2-\text{S}$ or $\text{C}=\text{N}-\text{CH}_2\text{CH}_2-\text{S}$), 5.33 (s, 1H, CH_2Cl_2), 6.89 (d, 2H, Aryl, $J_{\text{H}-\text{H}} = 3.2$ Hz), 7.33 (d, 2H, aryl, $J_{\text{H}-\text{H}} = 3.6$ Hz), 9.47 (s, 2H, $\text{N}=\text{CH}-$). ^1H NMR (399.78 MHz, $\text{DMSO}-d_6$, δ /ppm vs. TMS): 1.64 (s, 18H, $-\text{C}(\text{CH}_3)_3$), 3.77 (s, 6H, $\text{O}-\text{CH}_3$), 3.79 (br, 4H, $\text{C}=\text{N}-\text{CH}_2\text{CH}_2-\text{S}$ or $\text{C}=\text{N}-\text{CH}_2\text{CH}_2-\text{S}$), 4.60 (br, 4H, $\text{C}=\text{N}-\text{CH}_2\text{CH}_2-\text{S}$ or $\text{C}=\text{N}-\text{CH}_2\text{CH}_2-\text{S}$), 7.09 (d, 2H, aryl, $J_{\text{H}-\text{H}} = 3.2$ Hz), 7.18 (d, 2H, aryl, $J_{\text{H}-\text{H}} = 2.8$ Hz), 9.74 (s, 2H, $\text{N}=\text{CH}-$). IR (ATR, cm^{-1}): 880 ($\text{O}=\text{U}=\text{O}$ asymmetric stretching, ν_3), 1623 ($\text{C}=\text{N}$ stretching, $\nu_{\text{C}=\text{N}}$). Elemental analysis (%) calcd for $\text{UO}_2(\text{L}_\text{S}) \cdot 0.5\text{CH}_2\text{Cl}_2$ ($\text{C}_{28}\text{H}_{38}\text{N}_2\text{O}_6\text{S}_1\text{U}_1 \cdot 0.5\text{CH}_2\text{Cl}_2$): C, 42.20; H, 4.85; N, 3.45. Found: C 42.24; H, 4.79; N, 3.40. The obtained crystals were also suitable for the X-ray crystallography.

Methods

The ^1H NMR spectra were recorded by using JEOL ECX-400 (^1H : 399.78 MHz) NMR spectrometer. The chemical shifts of ^1H NMR were referenced to TMS ($\delta = 0$ ppm). The IR measurements were performed by JASCO FT/IR4700 equipped with a diamond ATR attachment. Elemental analyses were carried out by Yanaco MT-6 CHN elemental analyzer. Cyclic voltammetry (CV) measurements of $\text{UO}_2(\text{L}_\text{X})$ (1 mM) dissolved in DMSO containing 0.1 M tetra-*n*-butylammonium perchlorate (TBAP) were performed at 295 K under a dry Ar atmosphere by using BAS ALS660B electrochemical analyzer. A three-electrode system consisted of a Pt disk working electrode (diameter: 1.6 mm, surface area: 0.020 cm^2), a Pt wire counter electrode, and an $\text{Ag}^{0/+}$ reference electrode (0.1 M TBAP + 1 mM $\text{AgNO}_3/\text{CH}_3\text{CN}$). A ferrocene/ferrocenium ion redox couple ($\text{Fc}^{0/+}$) was taken as an external standard redox system. All samples were prepared under an inert Ar atmosphere. Dissolved oxygen gas in each sample solution was expelled by purging Ar gas for at least 10 min prior to starting the CV experiments. UV-vis-NIR spectroelectrochemical measurements in DMSO were performed with a JASCO V-770 spectrophotometer equipped with an optically transparent thin layer electrode (OTTLE) cell at 295 K.²⁴⁻²⁷ Its optical path length was 1.0×10^{-2} cm, which was calibrated spectrophotometrically.²² The three-electrode system was the same as that in the above electrochemical experiments with a replacement of the working electrode by a Pt gauze (80 mesh). The potential applied on OTTLE was controlled by BAS ALS660B. The absorption spectrum at each potential step was recorded after equilibration of the electrochemical reaction at the applied potential on the working electrode, which completed within 3 min. The sample solution in the OTTLE cell was prepared in a similar manner to that for the CV measurements.

Crystallographic analysis

The X-ray diffraction data of the well-shaped single crystals of $\text{UO}_2(\text{L}_\text{NH}) \cdot (\text{CH}_2\text{Cl}_2)$, $\text{UO}_2(\text{L}_\text{O}) \cdot (\text{C}_5\text{H}_5\text{N})$ and $\text{UO}_2(\text{L}_\text{S}) \cdot (\text{CH}_2\text{Cl}_2)$ were collected by a Rigaku XtaLAB mini II equipped with hybrid pixel array detector and graphite monochromated Mo K α radiation ($\lambda = 0.71073$ Å). Each sample was mounted on a MiTeGen

Dual Thickness MicroMounts, and located in the temperature-controlled N_2 gas flow. Intensity data were collected by taking oscillation photographs. Reflection data were corrected for both Lorentz and polarization effects. The structures were solved by the direct method and refined anisotropically by the SHELX program suite²⁸ for non-hydrogen atoms by full-matrix least-squares calculations. Each refinement was continued until all shifts were smaller than one-third of the standard deviations of the parameters involved. Hydrogen atoms were located at the calculated positions. All hydrogen atoms were constrained to ideal geometry with $\text{C}-\text{H} = 0.95$ Å. The thermal parameters of all hydrogen atoms were related to those of their parent atoms by $U(\text{H}) = 1.2U_{\text{eq}}(\text{C})$. All calculations were performed by using the Olex2 crystallographic software program package.²⁹ Crystallographic data of all complexes were summarized in Table S1,[†] and deposited with Cambridge Crystallographic Data Centre as supplementary publication no: CCDC 2177295 ($\text{UO}_2(\text{L}_\text{O}) \cdot (\text{C}_5\text{H}_5\text{N})$), 2177296 ($\text{UO}_2(\text{L}_\text{NH}) \cdot (\text{CH}_2\text{Cl}_2)$), and 2177297 ($\text{UO}_2(\text{L}_\text{S}) \cdot (\text{CH}_2\text{Cl}_2)$).

UV-vis titration

Sample solutions of $\text{H}_2\text{L}_\text{X}$ ($\text{X} = \text{NH, O, S}$, 0.1 mM) were prepared by mixing 3-*tert*-butyl-5-methoxysalicylaldehyde and the corresponding diamines in ethanol. The formation of $\text{H}_2\text{L}_\text{X}$ ($\text{X} = \text{NH, O, S}$) was checked by ^1H NMR spectroscopy (see Fig. S1[†]). Triethylamine (NET_3 , 0.4 mM) was added as a H^+ scavenger after the formation of $\text{UO}_2(\text{L}_\text{X})$. The total concentration of UO_2^{2+} was stepwise increased up to 0.12 mM ($0 \leq [\text{UO}_2^{2+}]/[\text{L}_\text{X}^{2-}] \leq 1.2$) by adding a feed solution of $\text{UO}_2(\text{NO}_3)_3 \cdot 6\text{H}_2\text{O}$ (10 mM) in ethanol. The UV-vis absorption spectrum at each increment step was recorded by JASCO V-770 spectrophotometer. During the whole titration experiment, temperature of the sample solution was kept at 293 K in a thermostat cell holder equipped with the spectrophotometer. The obtained titration series of the UV-vis absorption spectra was analyzed by HypSpec (version 1.1.33)³⁰ to determine conditional stability constants of $\text{UO}_2(\text{L}_\text{X})$ ($\text{X} = \text{NH, O, S}$) under the presence of 0.4 mM NET_3 in ethanol.

Theoretical calculations

Density functional theory (DFT) calculations were performed using Gaussian 16 program (Revision B.01)³¹ for characterization of $\text{UO}_2(\text{L}_\text{X})$ and the one-electron reduced complexes, $[\text{UO}_2(\text{L}_\text{X})]^-$ ($\text{X} = \text{NH, O, S}$). The atomic coordinates of $\text{UO}_2(\text{L}_\text{X})$ were taken from those experimentally-determined and were used for structure optimization. Hybrid DFT functional B3LYP³² was employed and solvent was modelled through a conductor-like polarized continuum model (CPCM) for DMSO (dielectric $\epsilon = 46.7$).³³ For uranium, Stuttgart-type small-core effective core potential (ECP) and corresponding basis set has been used.³⁴ The most diffuse basis functions on uranium with the exponent 0.005 (all s, p, d, and f type functions) were omitted as in previous studies.³⁵⁻³⁹ The 6-311G(d) basis sets were used for other elements (C, H, N, O, S). Vibrational frequency calculations at the same level of theory confirmed that no imaginary frequency was found to be present. Single-point calculations for energetic analysis were performed using the same condition.



NBO analysis were carried out by using the NBO 5.0 program.⁴⁰ The molecular structures of $[\text{UO}_2(\text{L}_X)]^-$ were taken from those of $\text{UO}_2(\text{L}_X)$ determined experimentally and were optimized after addition of a single negative charge and doublet spin degeneracy to assume the one-electron reduction using the same condition. The Mulliken spin-density plots were illustrated by GaussView 6.1.⁴¹

Results and discussion

Synthesis and structure determination of $\text{UO}_2(\text{L}_X)$ ($\text{X} = \text{NH, O, S}$)

Each ligand was synthesized through a condensation reaction between a 3-*tert*-butyl-5-methoxysalicylaldehyde and the corresponding diamine in ethanol, and further reacted with one equivalent of $\text{UO}_2(\text{NO}_3)_2 \cdot 6\text{H}_2\text{O}$ to afford $\text{UO}_2(\text{L}_X)$. These complexes were yielded as red microcrystalline solids, which were recrystallized from appropriate solvent mixtures to obtain single crystals suitable for X-ray structure determination. The IR peaks of $[\text{O} \equiv \text{U} \equiv \text{O}]^{2+}$ asymmetric stretching (ν_3) and C=N stretching ($\nu_{\text{C}=\text{N}}$) of $\text{UO}_2(\text{L}_X)$ were observed at around 860–880 and 1630 cm^{-1} , respectively. The elemental analysis for $\text{UO}_2(\text{L}_X)$ well-agreed with the expected chemical formulae of them.

The molecular structures of $\text{UO}_2(\text{L}_X)$ were determined by single crystal X-ray diffraction (SCXRD). The resulting molecular structures of $\text{UO}_2(\text{L}_X)$ are shown in Fig. 2 and S2.[†] The selected bond lengths of them are summarized in Table 1. As a general trend, UO_2^{2+} in $\text{UO}_2(\text{L}_X)$ is five-coordinated in its equatorial plane to give a pentagonal bipyramidal coordination geometry as expected in Fig. 1(b), which is typically found in UO_2^{2+} complexes.^{21,22}

The $\text{U} \equiv \text{O}_{\text{ax}}$ bond lengths of UO_2^{2+} in $\text{UO}_2(\text{L}_X)$ (U(1)-O(1), U(1)-O(2)) are 1.78–1.79 Å, which is similar to those in UO_2^{2+} complexes reported previously.^{21,22} Herein, we introduced *tert*-butyl groups at the *ortho*-positions of the phenolate moieties in each system to control the structure of the ligand after coordination to UO_2^{2+} . To avoid steric collision between these bulky groups in $\text{UO}_2(\text{L}_X)$, two phenolate moieties are forced to be present in the opposite sides of the equatorial plane of UO_2^{2+} (Fig. 2 and S2[†]). Such a twisted structure of a planar pentadentate ligand was also observed in the saldien-type ligands (e.g., Fig. 1(a)) we reported previously.^{21,22}

The bond angles around X are strongly affected by the difference in X. The mean bond angle of C(9)-N(3)-C(10), C(9)-

Table 1 Selected bond lengths (Å) of $\text{UO}_2(\text{L}_X)$ ($\text{X} = \text{NH, O, S}$)

	$\text{UO}_2(\text{LNH})$	$\text{UO}_2(\text{LO})$	$\text{UO}_2(\text{LS})$
U-O(1)	1.793(2)	1.792(2)	1.776(5)
U-O(2)	1.787(2)	1.790(2)	1.778(5)
U-O(3)	2.238(2)	2.239(2)	2.241(6)
U-O(4)	2.239(2)	2.239(2)	2.231(5)
U-N(1)	2.535(3)	2.523(3)	2.543(7)
U-N(2)	2.554(2)	2.531(3)	2.542(6)
U-X	2.594(5)	2.581(3)	2.981(2)
C(1)-O(3)	1.342(3)	1.332(3)	1.34(1)
C(18)-O(4)	1.333(3)	1.334(3)	1.34(1)

N(3)-U(1) and C(10)-N(3)-U(1) in $\text{UO}_2(\text{LNH})$ is 111° , which is close to the ideal value (109.5°) of the tetrahedral coordination around N, showing its sp^3 character. Note that the N-H moiety in $\text{UO}_2(\text{LNH})$ forms a hydrogen bond with the axial O of UO_2^{2+} of the neighboring complexes (D···A: 3.15 Å, D-H: 1.00 Å, H···A: 2.210 Å, D-H···A: 154.9°). Nevertheless, there seems to be little effect on the structure of this UO_2^{2+} complex, because the similar bond angles around N was also observed in $\text{UO}_2(-t\text{Bu},\text{MeO}^-\text{Me}\text{sal}\text{dien})$ (109° , see Fig. 1). The mean bond angles around X in $\text{UO}_2(\text{LO})$ and $\text{UO}_2(\text{LS})$ are 120° and 98° . Moreover, the deviation of X from the mean planes defined by U1, N1, N2, O3, and O4 in $\text{UO}_2(\text{LS})$ (0.489 Å) is larger than those of $\text{UO}_2(\text{LNH})$ (0.261 Å) and $\text{UO}_2(\text{LO})$ (0.116 Å). Such a difference would be related to the bonding nature and steric factor of these X atoms. However, it is difficult at this moment to clearly describe in detail how the hardness/softness of X affects such a structural trend. Hence, we decided to focus on the bond lengths around X as another structural parameter directly affected by the coordination strength.

In the $\text{UO}_2(\text{L}_X)$ complexes studied here, the bond lengths between U and the phenolic O (U(1)-O(3), U(1)-O(4)) are 2.23–2.24 Å regardless of difference in X. This is also the case for those between U and the imino N (U(1)-N(1), U(1)-N(2), 2.52–2.55 Å). In contrast, the U(1)-X bond lengths depend on X. The U(1)-N(3) distance of $\text{UO}_2(\text{LNH})$ is 2.594(5) Å, which is slightly longer than the corresponding interaction in $\text{UO}_2(\text{LO})$ (U(1)-O(5) = 2.581(3) Å). These bond lengths are commonly found in the previous reports.^{21,22} The U(1)-S(1) distance in $\text{UO}_2(\text{LS})$ is significantly longer than the others. However, the U(1)-S(1) distance of $\text{UO}_2(\text{LS})$ is still shorter than the sum of van der Waals radii of U and S (2.3 Å + 1.8 Å = 4.1 Å),⁴² suggesting that chemical bonding interaction is certainly present between U(1)

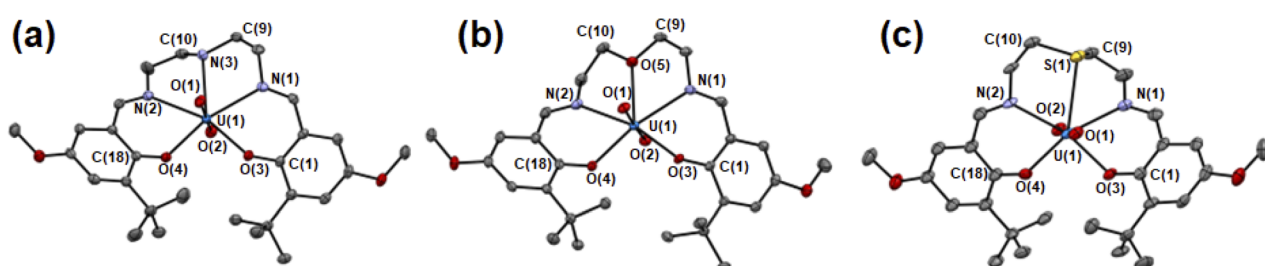


Fig. 2 ORTEP views of $\text{UO}_2(\text{LNH})$ (a), $\text{UO}_2(\text{LO})$ (b), $\text{UO}_2(\text{LS})$ (c). Ellipsoids are at 50% probability level. Hydrogen atoms and solvent molecules were omitted for clarity.



and S(1) in this complex. Indeed, the U(1)-S(1) distance of $\text{UO}_2(\text{L}_\text{S})$ (2.981(2) Å) is close to the U-S bond lengths in UO_2^{2+} -thioether complexes reported previously (2.96–3.02 Å).^{2,43,44} The observed structural parameters of the U-X interactions in $\text{UO}_2(\text{L}_\text{X})$ are quite common in uranyl complexes having X atom coordination reported so far.^{2,21,22,43,44} Therefore, $\text{UO}_2(\text{L}_\text{X})$ studied here are suitable for exploring impacts of X in the coordination chemistry of UO_2^{2+} .

It could be misleading to discuss the strengths of the U-X bonding interactions solely on the basis of the observed bond lengths, because the sizes of N, O and S are different from each other. The bond strengths between two atoms can be normalized by reduction in an interaction distance (R_{UX}) derived from the sum of van der Waals radii and an actual bond length between U and X as shown in eqn (1).^{45–47}

$$R_{\text{UX}} = (d_{\text{UX}})/(r_{\text{U}} + r_{\text{X}}) \quad (1)$$

where r_{U} and r_{X} are van der Waals radii of U and X, respectively. d_{UX} is the U-X bond length of $\text{UO}_2(\text{L}_\text{X})$ determined by SCXRD.^{45–47} Based on this definition, greater R_{UX} implies weaker U-X bond (*vice versa*). As a result, R_{UX} of $\text{UO}_2(\text{L}_\text{NH})$ is 0.665, which is close to that of $\text{UO}_2(\text{L}_\text{O})$ (0.670). This implies that the bond strengths of U(1)-N(3) in $\text{UO}_2(\text{L}_\text{NH})$ and U(1)-O(5) in $\text{UO}_2(\text{L}_\text{O})$ are similar to each other. In contrast, R_{UX} of $\text{UO}_2(\text{L}_\text{S})$ is 0.727, which is significantly greater than those of $\text{UO}_2(\text{L}_\text{NH})$ and $\text{UO}_2(\text{L}_\text{O})$. Hence, the U(1)-S(1) bond strength of $\text{UO}_2(\text{L}_\text{S})$ is supposed to be weaker than the U-X ones in $\text{UO}_2(\text{L}_\text{NH})$ and $\text{UO}_2(\text{L}_\text{O})$. Consequently, the bond strength of U-X interactions follows $\text{U-O} \approx \text{U-NH} > \text{U-S}$. As widely accepted in the HSAB principle, the hardness of X moiety follows $\text{O} > \text{NH} > \text{S}$.^{14,15} Therefore, the trend of U-X bond strengths of $\text{UO}_2(\text{L}_\text{X})$ cannot be explained only by the HSAB principle, while the bond strength of U(1)-S(1) of $\text{UO}_2(\text{L}_\text{S})$ is certainly weaker than others. Note that all R_{UX} of $\text{UO}_2(\text{L}_\text{X})$ presented here are much smaller than those of noncovalent intermolecular interactions such as $\text{Cl}\cdots\text{X}$ and hydrogen bonds reported previously, where $R = 0.98\text{--}0.80$.^{45–47} Therefore, a coordination bond is certainly formed between U and X in each $\text{UO}_2(\text{L}_\text{X})$.

Thermodynamic stability of $\text{UO}_2(\text{L}_\text{X})$ (X = NH, O, S)

In the crystal structures of $\text{UO}_2(\text{L}_\text{X})$ (X = NH, O, S), the U-X bond strength depends on the difference in X. Therefore, there would also be some impact on the thermodynamic stability of $\text{UO}_2(\text{L}_\text{X})$. To confirm this issue, we investigated the complexation of UO_2^{2+} and L_X^{2-} in ethanol by spectrophotometric titration. Fig. 3 shows the UV-vis absorption spectra recorded at different total concentration ratios between UO_2^{2+} and L_X^{2-} represented by $C_{\text{U}}/C_{\text{L}}$. Note that these titration experiments were conducted under the presence of 0.4 mM NET_3 employed as a H^+ scavenger after the formation of $\text{UO}_2(\text{L}_\text{X})$.

In all titration series shown in Fig. 3, the absorbance at 370 nm and 425 nm increased with an increase in $C_{\text{U}}/C_{\text{L}}$. Simultaneously, the absorption intensity at 350 nm decreased. The isosbestic points were clearly observed, indicating that the complexation equilibrium between UO_2^{2+} and L_X^{2-} only takes place in each system. As shown in the insets of Fig. 3(a) and (b), the absorbance at 370 nm tends to be saturated at $C_{\text{U}}/C_{\text{L}} = 1.0$, indicating that $\text{UO}_2(\text{L}_\text{NH})$ and $\text{UO}_2(\text{L}_\text{O})$ are almost quantitatively formed. On the other hand, such a trend is equivocal for X = S (Fig. 3(c)), implying that the weaker coordination of L_S^{2-} .

To estimate the conditional stability constants ($\beta_{\text{X}} = [\text{UO}_2(\text{L}_\text{X})]/([\text{UO}_2^{2+}][\text{L}_\text{X}^{2-}])$) of $\text{UO}_2(\text{L}_\text{X})$ (X = NH, O, S) in ethanol containing NET_3 (0.4 mM), the spectral series of Fig. 3 were analyzed by HypSpec program.³⁰ As a result, $\log \beta_{\text{X}}$ of $\text{UO}_2(\text{L}_\text{X})$ for X = NH, O, and S are estimated to be 10 ± 1 , 7.24 ± 0.02 , and 5.2 ± 0.1 , respectively. Since all the coordinating atoms except for X are common in the studied systems, the difference in $\log \beta_{\text{X}}$ observed here can be ascribed to the difference in affinity of X with UO_2^{2+} . As widely-accepted in the HSAB principle, the hardness of X atoms follows $\text{O} > \text{NH} > \text{S}$.^{14,15} However, $\log \beta_{\text{X}}$ of $\text{UO}_2(\text{L}_\text{X})$ decrease in the order of $\text{UO}_2(\text{L}_\text{NH}) > \text{UO}_2(\text{L}_\text{O}) > \text{UO}_2(\text{L}_\text{S})$, which is difficult to be rationalized only by the HSAB principle. To understand this trend, we focus on difference in basicity of X in L_X^{2-} . The pK_a values of protonated diethylamine ($(\text{CH}_3\text{CH}_2)_2\text{NH}_2^+$), dimethyl ether ($(\text{CH}_3)_2\text{OH}^+$), and dimethyl thioether ($(\text{CH}_3)_2\text{SH}^+$) are 11.0 (ref. 48), -3.8 (ref. 48), and -5.4 (ref. 48), respectively, which is exactly in line with the order of $\log \beta_{\text{X}}$.

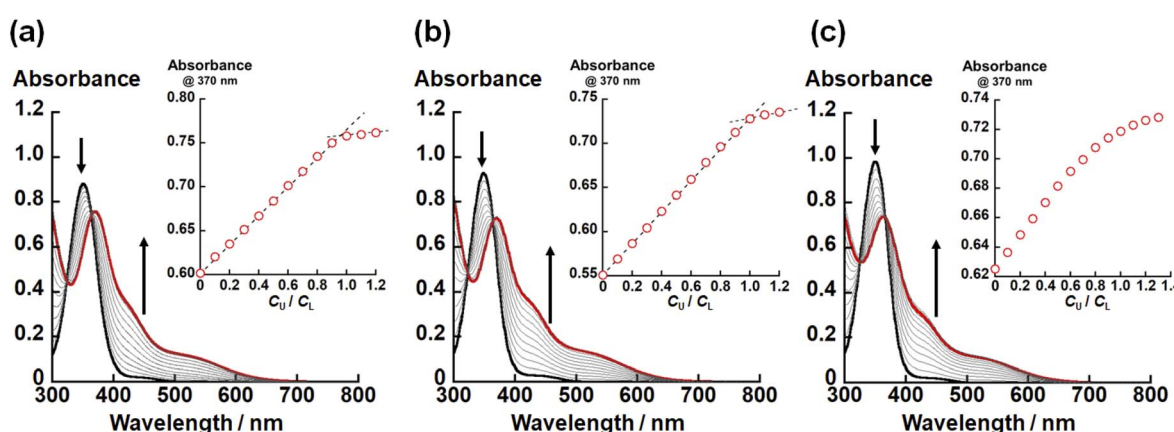


Fig. 3 UV-vis absorption spectra of the ethanol solutions of (a) L_NH^{2-} , (b) L_O^{2-} and (c) L_S^{2-} at different total UO_2^{2+} concentrations under the presence of 0.4 mM NET_3 . Total concentration of L_X^{2-} : 0.1 mM. Black and red lines are spectra of $C_{\text{U}}/C_{\text{L}} = 0$ and 1.0, respectively. Insets: plots of absorbance at 370 nm with an increase in $C_{\text{U}}/C_{\text{L}}$.



of $\text{UO}_2(\text{L}_\text{X})$ described above. Therefore, the basicity of X atom would also provide some contribution to the thermodynamic stability of $\text{UO}_2(\text{L}_\text{X})$. At this moment, it is still too early to verify linear free energy relationship between $\log \beta_\text{X}$ and pK_a .

To further elucidate the nature of U-X bonds in $\text{UO}_2(\text{L}_\text{X})$, we carried out DFT calculations of $\text{UO}_2(\text{L}_\text{X})$, followed by the natural bond orbital (NBO) analysis. The molecular structures of $\text{UO}_2(\text{L}_\text{X})$ were taken from those of $\text{UO}_2(\text{L}_\text{X})$ determined by X-ray crystallography, and were optimized with B3LYP method.³² The optimized structures of $\text{UO}_2(\text{L}_\text{X})$ are shown in Fig. S4,[†] and selected bond lengths are summarized in Table S2.[†] All the bond distances well agree with those determined crystallographically (Table 1). Table S3[†] summarizes natural charges and Wiberg bond indices (WBI)^{17,18,40} of center U and coordinating atoms in the optimized structures.

No significant differences were found in the natural charge on the axial and equatorial coordinating atoms except for X. Both N(3) in $\text{UO}_2(\text{L}_\text{NH})$ (-0.646) and O(5) in $\text{UO}_2(\text{L}_\text{O})$ (-0.565) have negative natural charges, indicating that the center U and X atoms interact electrostatically. In contrast, the natural charge of S(1) in $\text{UO}_2(\text{L}_\text{S})$ is positive ($+0.326$), implying that the electrostatic attraction between U and S is little expectable despite significant penetration between these atoms in $\text{UO}_2(\text{L}_\text{S})$ within the sum of van der Waals radii as described above. To provide a rationale for the U-S bonding interaction experimentally observed, bond orders of U-X interactions were estimated in terms of WBI. As a result, some covalency was detected in the U-S bond of $\text{UO}_2(\text{L}_\text{S})$ as pronounced by $\text{WBI} = 0.471$, which is significantly larger than those of the other U-X bonds ($\text{WBI} = 0.277\text{--}0.345$). Therefore, the bonding interaction between U and S of $\text{UO}_2(\text{L}_\text{S})$ is rather covalent, while it is somewhat weakened by the electrostatic repulsion between these positively charged atoms. The significant covalency of the U-S interaction compared with the electrostatic characters in U-NH and U-O would be a typical manifestation of the HSAB principle. In connection with this, N is usually considered to be softer than O, while the stability of $\text{UO}_2(\text{L}_\text{NH})$ is greater than $\text{UO}_2(\text{L}_\text{O})$ despite the hardness of UO_2^{2+} . The stronger basicity of NH provides an additional effect to strengthen the U-NH bond compared with that of U-O.

Electrochemistry and spectroelectrochemistry of $\text{UO}_2(\text{L}_\text{X})$ ($\text{X} = \text{NH, O, S}$)

As mentioned above, X strongly affects the thermodynamic stability of $\text{UO}_2(\text{L}_\text{X})$. Recently, we have reported that the redox potential of $\text{UO}_2(\text{R}_1\text{R}_2\text{---}^\text{Me}\text{salphen})$ (Fig. 1(a)) is significantly governed by substitution at R_1 and R_2 positions. Therefore, we expect that the difference in X may also vary the redox potentials of $\text{UO}_2(\text{L}_\text{X})$. To clarify this point, the electrochemical measurements of $\text{UO}_2(\text{L}_\text{X})$ in DMSO were carried out. Fig. 4 shows the obtained cyclic voltammograms of $\text{UO}_2(\text{L}_\text{X})$, where a couple of cathodic (E_{pc}) and anodic peaks (E_{pa}) has been observed. These redox waves are reproducible even in multiple scanned cyclic voltammograms recorded at the potential sweep rate (ν) of 100 mV s^{-1} , indicating that the reduction product at E_{pc} undergoes no successive reactions, and is fully reoxidized to $\text{UO}_2(\text{L}_\text{X})$ at E_{pa} (Fig. S6[†]). The peak potential separation ($E_{\text{pa}} - E_{\text{pc}}$)

tends to increase (111–490 mV) with increasing ν from 50 mV s^{-1} to 500 mV s^{-1} (Fig. S7 and Tables S4–S6[†]), implying that these redox systems of $\text{UO}_2(\text{L}_\text{X})$ are quasireversible. Even after careful survey of the DFT calculations described later, we, however, could not find any critical rationales for the differences in the electrochemical reversibility of these systems. Anyway, the peak potential separations ($E_{\text{pa}} - E_{\text{pc}}$, see Table S6 in ESI[†]) of $\text{UO}_2(\text{L}_\text{S})$ were also much greater than the theoretical value of a reversible system (59 mV). Therefore, all the systems studied here are regarded to be electrochemically irreversible. Although we do not have unequivocal explanation for the above points at this moment, solvation structures around these uranyl complexes could be largely modified through the electron transfer. Note that all the redox reactions are chemically reversible as demonstrated by occurrence of the isosbestic points in the spectroelectrochemical experiments shown in Fig. 5, S8 and S9.[†] The diffusion coefficients (D_0) of $\text{UO}_2(\text{L}_\text{NH})$, $\text{UO}_2(\text{L}_\text{O})$, and $\text{UO}_2(\text{L}_\text{S})$

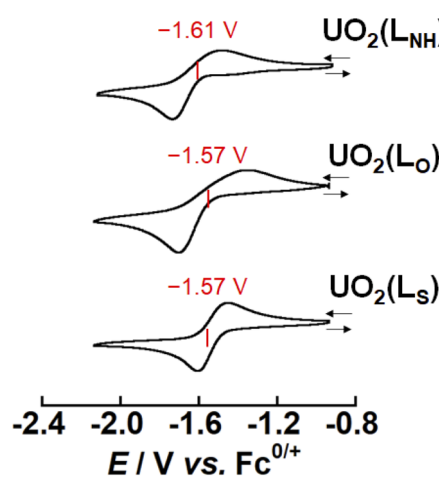


Fig. 4 Cyclic voltammograms for the redox couples of $\text{UO}_2(\text{L}_\text{X})$ ($\text{X} = \text{NH, O, S}$) in DMSO at 295 K. Concentration of the complex was adjusted to 1 mM and tetra-*n*-butylammonium perchlorate (0.1 M) was used as a supporting electrolyte. Scan rates are 100 mV s^{-1} .

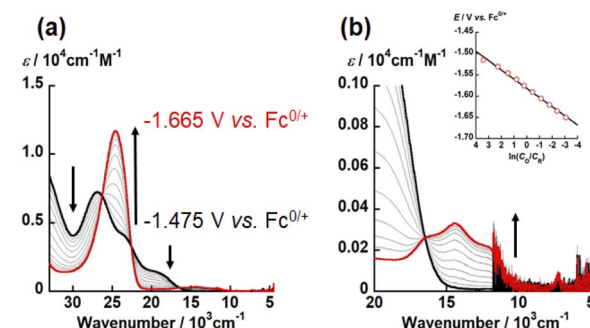


Fig. 5 UV-vis-NIR spectral change of electrochemical reduction of $\text{UO}_2(\text{L}_\text{O})$ recorded at different applied potentials from -1.475 V to -1.665 V vs. $\text{Fc}^{0+/}$ (potential step: 0.015 V) in DMSO with 0.1 M TBAP at 295 K. Black and red bold curves represent absorption spectra of $\text{UO}_2(\text{L}_\text{O})$ and $[\text{UO}_2(\text{L}_\text{O})]^-$, respectively. Wavenumber regions: (a) $33\ 333\text{--}4500 \text{ cm}^{-1}$, (b) $20\ 000\text{--}4500 \text{ cm}^{-1}$. Inset: Nernstian plot calculated from absorbance at $24\ 630 \text{ cm}^{-1}$.



in these systems at 295 K were estimated as 1.6×10^{-6} , 1.8×10^{-6} and $8.1 \times 10^{-7} \text{ cm}^2 \text{ s}^{-1}$, respectively, where the redox reactions observed in Fig. 4 were assumed to be electrochemically irreversible.⁴⁹ As summarized in Tables S4–S6,[†] the formal potential $E^{\circ'}$ ($= (E_{\text{pc}} + E_{\text{pa}})/2$) of each $\text{UO}_2(\text{L}_X)$ is around -1.60 V vs. $\text{Fc}^{0+/}$ with regardless of ν , and also seems not to be largely affected by X . The $E^{\circ'}$ value of $\text{UO}_2(\text{L}_{\text{NH}})$ well agrees with that of its analogue, $\text{UO}_2(t\text{Bu}_2\text{MeO}-\text{Me}\text{salphen})$, we reported previously (-1.60 V vs. $\text{Fc}^{0+/}$ in DMSO).^{21,22} Therefore, the coordinating L_X^{2-} would not have strong contribution to the redox events of $\text{UO}_2(\text{L}_X)$. From these results, we assume that the redox centers of all $\text{UO}_2(\text{L}_X)$ are the UO_2^{2+} moiety. However, cyclic voltammograms does not provide any detailed information about the reductant of $\text{UO}_2(\text{L}_X)$. Hence, we carried out the spectroelectrochemical measurements and theoretical calculations to further understand the redox chemistry of $\text{UO}_2(\text{L}_X)$.

To determine the electron stoichiometry (n) in the reduction of $\text{UO}_2(\text{L}_X)$, the spectroelectrochemical measurements were performed. The UV-vis-NIR spectra of each system were recorded at different potentials (E). Fig. 5, S8 and S9[†] show the obtained spectral variations at $\text{X} = \text{O}$, NH , and S , respectively. As a general trend, the absorption bands of $\text{UO}_2(\text{L}_X)$ around $30\,000$ and $20\,000 \text{ cm}^{-1}$ gradually decreased with decreasing E , while new absorption bands appeared around $25\,000$ and $15\,000 \text{ cm}^{-1}$. Moreover, isosbestic points were clearly observed, indicating that the redox equilibria of $\text{UO}_2(\text{L}_X)$ only take place in the current potential ranges. Using the absorbance at $24\,630$ or $24\,876 \text{ cm}^{-1}$, the concentration ratio ($C_{\text{O}}/C_{\text{R}}$) between the oxidant ($\text{UO}_2(\text{L}_X)$) and its reductant at each E was calculated. The relationship between $C_{\text{O}}/C_{\text{R}}$ and E should follow the Nernstian equation, eqn (2).

$$E = E^{\circ'} + (RT/nF)\ln(C_{\text{O}}/C_{\text{R}}) \quad (2)$$

where $E^{\circ'}$, R , T , and F are the formal potential, the gas constant ($8.314 \text{ J mol}^{-1} \text{ K}^{-1}$), the absolute temperature, and the Faraday constant ($96\,485 \text{ C mol}^{-1}$), respectively. The slope and intercept of the linear relationship between E and $\ln(C_{\text{O}}/C_{\text{R}})$ (insets of Fig. 5(b), S8(b) and S9(b)[†]) allow to determine n and $E^{\circ'}$ of the

redox reactions of $\text{UO}_2(\text{L}_X)$. The estimated n values of $\text{UO}_2(\text{L}_X)$ are close to unity (Table S7[†]), indicating that the reduction of $\text{UO}_2(\text{L}_X)$ affords $[\text{UO}_2(\text{L}_X)]^-$. The $E^{\circ'}$ values estimated from the spectroelectrochemical measurements (Table S7[†]) agree with those observed in the CV measurements (Tables S4–S6[†]).

UV-vis-NIR spectra of $\text{UO}_2(\text{L}_X)$ and $[\text{UO}_2(\text{L}_X)]^-$ in DMSO were summarized in Fig. 6. The spectral features of all $\text{UO}_2(\text{L}_X)$ are quite similar to each other. All $\text{UO}_2(\text{L}_X)$ showed characteristic bands around $28\,000$ and $24\,000 \text{ cm}^{-1}$. These absorption bands were also observed in UO_2^{2+} complexes with Schiff base ligands, and can be assigned to the $\pi-\pi^*$ transition bands of Schiff base ligands.^{21,22} Therefore, the difference in X leads to no significant differences in the electronic structures of $\text{UO}_2(\text{L}_X)$.

Even after the reduction, $[\text{UO}_2(\text{L}_X)]^-$ with different X commonly have the intense bands at around $25\,000 \text{ cm}^{-1}$ with $\epsilon \sim 10^4 \text{ M}^{-1} \text{ cm}^{-1}$ and weak bands at $16\,400$, $14\,500$, $12\,200$ and 7200 cm^{-1} with $\epsilon \sim 10^2 \text{ M}^{-1} \text{ cm}^{-1}$ (Fig. 6). Note that $[\text{UO}_2(\text{L}_{\text{NH}})]^-$ has a characteristic band at 5200 cm^{-1} , although this absorption is not clearly observed in $[\text{UO}_2(\text{L}_\text{O})]^-$ and $[\text{UO}_2(\text{L}_\text{S})]^-$ (Fig. 6). The absorption bands at around $25\,000$, $16\,400$, $14\,500$, $12\,200$ and 7200 cm^{-1} are generally observed in $\text{U}^{\text{V}}\text{O}_2^+$ complexes with Schiff base ligands as reported previously.^{21,22} The intense absorption at $25\,000 \text{ cm}^{-1}$ is assigned to a $\pi-\pi^*$ transition in the Schiff base ligands and/or a ligand-to-metal charge transfer (LMCT).^{21,22} In accordance with TD-DFT calculation,^{21,22} the absorption band at $16\,400 \text{ cm}^{-1}$ is attributable to a metal-to-ligand charge transfer (MLCT) from a $5f\delta_u$ orbital of the U^{5+} center to the π^* orbital of the coordinating ligand. Finally, those at $14\,500$, $12\,200$ and 7200 cm^{-1} are ascribed to the f-f transitions arising from the $5f^4$ electron configuration of U^{5+} .^{21,22,35} $[\text{UO}_2(\text{L}_{\text{NH}})]^-$ only exhibited the absorption band at 5200 cm^{-1} attributable to another f-f transition,^{21,22,35} while this is not the case for the others studied here. As a matter of fact, this transition is not always clearly observable as we reported previously.²² To theoretically support occurrence of $\text{U}^{\text{V}}\text{O}_2^+$ in each $[\text{UO}_2(\text{L}_X)]^-$, we further performed DFT calculations of $[\text{UO}_2(\text{L}_X)]^-$.

Initially, the molecular structures of $[\text{UO}_2(\text{L}_X)]^-$ in DMSO were taken from those of $\text{UO}_2(\text{L}_X)$ determined by the X-ray

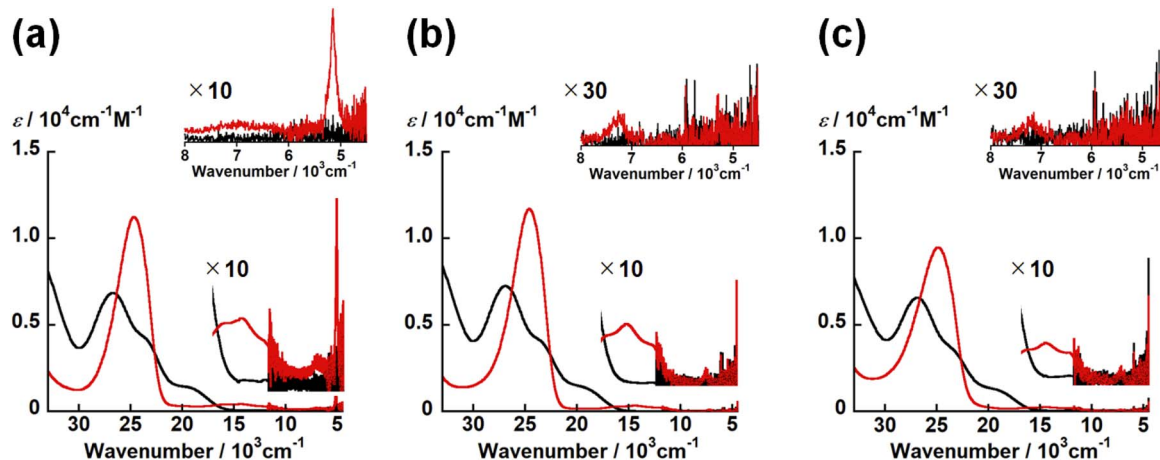


Fig. 6 UV-vis-NIR spectrum of $\text{UO}_2(\text{L}_X)$ (black) and one-electron reduced complexes $[\text{UO}_2(\text{L}_X)]^-$ (red) in DMSO containing 0.1 M tetra-*n*-butylammonium perchlorate at 295 K . $[\text{UO}_2(\text{L}_{\text{NH}})]^{-/0}$ (a), $[\text{UO}_2(\text{L}_\text{O})]^{-/0}$ (b) and $[\text{UO}_2(\text{L}_\text{S})]^{-/0}$ (c). Inset: expended views of NIR region.



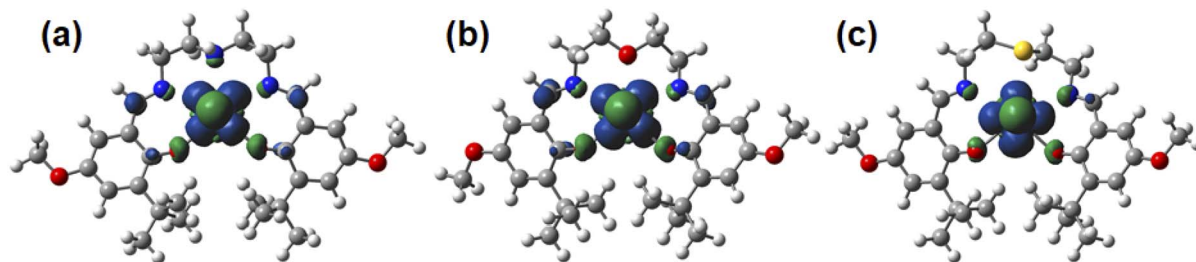


Fig. 7 Spin-density plots of $[\text{UO}_2(\text{L}_{\text{NH}})]^-$ (a), $[\text{UO}_2(\text{L}_\text{O})]^-$ (b), $[\text{UO}_2(\text{L}_\text{S})]^-$ (c). Spin density values of U atom are 1.09 for $[\text{UO}_2(\text{L}_{\text{NH}})]^-$, 1.09 for $[\text{UO}_2(\text{L}_\text{O})]^-$, 1.12 for $[\text{UO}_2(\text{L}_\text{S})]^-$.

crystal structure and were optimized after addition of a single negative charge and doublet spin degeneracy to assume the one-electron reduction. The optimized structures of $[\text{UO}_2(\text{L}_\text{X})]^-$ were shown in Fig. S10[†] and the selected structural parameters are summarized in Table S2.[†]

The $\text{U}\equiv\text{O}_{\text{ax}}$ bond lengths of $[\text{UO}_2(\text{L}_\text{X})]^-$ are 1.86 \AA , which are *ca.* 0.08 \AA longer than those of the corresponding $\text{UO}_2(\text{L}_\text{X})$ determined by SCXRD (Table 1). These $\text{U}\equiv\text{O}_{\text{ax}}$ bond lengths are very similar to those of the $\text{U}^{\text{V}}\text{O}_2^+$ complexes with bis(phenolate) ligands ($1.851(7)$ – $1.868(8)\text{ \AA}$).⁵⁰ The U–O bond lengths between U atom and phenolic O of $[\text{UO}_2(\text{L}_\text{X})]^-$ are *ca.* 0.15 \AA longer than those of the corresponding $\text{UO}_2(\text{L}_\text{X})$ (Table 1). These U–O bond elongations indicate that these bond strengths are weakened by a decrease in the positive charge of U through the reduction from $\text{U}^{\text{VI}}\text{O}_2^{2+}$ to $\text{U}^{\text{V}}\text{O}_2^+$. Actually, an unpaired electron of $[\text{UO}_2(\text{L}_\text{X})]^-$ is exclusively localized in the center U as shown in the Mulliken spin density surfaces (Fig. 7), clearly indicating that these reduced complexes are of $\text{U}^{\text{V}}\text{O}_2^+$ regardless of difference in X. Consequently, the X moiety does not largely affect the redox chemistry of $[\text{UO}_2(\text{L}_\text{X})]^{-0}$.

Conclusions

In this study, $\text{UO}_2(t\text{Bu,MeO-saldien-X})$ ($\text{UO}_2(\text{L}_\text{X})$; X = NH, O, S) were synthesized and structurally characterized to discuss impacts of the heteroatoms (X) to the coordination chemistry of UO_2^{2+} . The crystal structures of $\text{UO}_2(\text{L}_\text{X})$ showed the five-coordinated UO_2^{2+} with L_X^{2-} in the equatorial plane. The $\text{U}\equiv\text{O}_{\text{ax}}$ bond length of UO_2^{2+} and the bond length between U and phenolic O are not affected by the difference in X. On the other hand, the U–X bond length increases in the order of $\text{UO}_2(\text{L}_\text{O}) < \text{UO}_2(\text{L}_{\text{NH}}) < \text{UO}_2(\text{L}_\text{S})$. After taking into account the differences in the atomic size of X, the normalized U–X bond strength in $\text{UO}_2(\text{L}_\text{X})$ was found to follow $\text{U–O} \approx \text{U–NH} > \text{U–S}$. While the U–O and U–NH bond strengths are similar to each other, the weaker U–S interaction can be explained by the HSAB principle. The logarithmic conditional stability constant ($\log \beta_\text{X}$) of $\text{UO}_2(\text{L}_\text{X})$ in ethanol containing 0.4 mM NET_3 decreases in the order of $\text{UO}_2(\text{L}_{\text{NH}})$ ($\log \beta_{\text{NH}} = 10$) $> \text{UO}_2(\text{L}_\text{O})$ ($\log \beta_{\text{O}} = 7.24$) $> \text{UO}_2(\text{L}_\text{S})$ ($\log \beta_{\text{S}} = 5.2$). This trend cannot be explained only by the HSAB principle, but rather follows the order of basicity of X. The theoretical calculations of $\text{UO}_2(\text{L}_\text{X})$ suggested that the ionic character of U–X bonds decreases in the order of U–NH > U–O > U–S. In contrast, the covalency increases as U–O < U–NH < U–S.

No significant differences were found in the electrochemistry of $\text{UO}_2(\text{L}_\text{X})$ with different X in terms of $E^{\text{o'}}$ and U-centered redox reaction. As demonstrated in this work, a UO_2^{2+} -ligand bond strength does not always follow the HSAB principle, but is also affected by other factors such as Lewis basicity and balance between ionic and covalent interactions of donating atoms to the center metal. These points should be more carefully considered to design molecular structures of ligands suitable for hydro-metallurgical separations of metal ions of interest.

Author contributions

T. T. devised the main conceptual ideas, carried out all experiments, and wrote the manuscript in consultation with K. T. K. T. supervised this project, discussed all experimental results with T. T., and edited the manuscript. All authors have given approval to the final version of the manuscript.

Conflicts of interest

There are no conflicts to declare.

Acknowledgements

The authors thank Prof. Dr Satoru Tsushima of Institute of Resource Ecology, Helmholtz-Zentrum Dresden-Rossendorf (HZDR), for supporting the DFT calculation. This work was supported in part by Grants-in-Aid for Scientific Research (No. 20H02663 to K. T., and 21J11942 to T. T.), JAEA Nuclear Energy S&T and Human Resource Development Project through concentrating wisdom Grant Number JPJA19P19209861.

Notes and references

- 1 U. Casellato, M. Vidali and P. A. Vigato, *Coord. Chem. Rev.*, 1979, **28**, 231–277.
- 2 M. Ephritikhine, *Coord. Chem. Rev.*, 2016, **319**, 35–62.
- 3 B. J. Thamer, *J. Am. Chem. Soc.*, 1957, **79**, 4298–4305.
- 4 E. Bullita, P. Guerriero, S. Tamburini, P. A. Vigato, J. C. Dupuy, M. Prevost, R. Bonora and L. Marchesini, *Mater. Chem. Phys.*, 1992, **31**, 181–198.
- 5 S. Chattaraj, A. Bhattacharyya and B. Sadhu, *Inorg. Chem.*, 2021, **60**, 15351–15363.



6 K. E. Gutowski, V. A. Cocalia, S. T. Griffin, N. J. Bridges, D. A. Dixon and R. D. Rogers, *J. Am. Chem. Soc.*, 2007, **129**, 526–536.

7 X. Li, Z. Zhang, L. R. Martin, S. Luo and L. Rao, *Inorg. Chem.*, 2018, **57**, 7684–7693.

8 B. G. Vats, A. Bhattacharyya, K. Sanyal, M. Kumar, J. S. Gamare and S. Kannan, *Inorg. Chem.*, 2021, **60**, 17529–17536.

9 C. Berger, C. Marie, D. Guillaumont, C. Tamain, T. Dumas, T. Dirks, N. Boubals, E. Acher, M. Laszczyk and L. Berthon, *Inorg. Chem.*, 2020, **59**, 1823–1834.

10 Y. Zhang, W. Duan, Y. Yang, T. Jian, Y. Qiao, G. Ren, N. Zhang, L. Zheng, W. Yan, J. Wang, J. Chen, S. G. Minasian and T. Sun, *Inorg. Chem.*, 2022, **61**, 92–104.

11 Y. Sasaki and S. Tachimori, *Solvent Extr. Ion Exch.*, 2002, **20**, 21–34.

12 K. Takao and Y. Ikeda, *Eur. J. Inorg. Chem.*, 2020, **36**, 3443–3459.

13 T. Mizumachi, M. Sato, M. Kaneko, T. Takeyama, S. Tsushima and K. Takao, *Inorg. Chem.*, 2022, **61**, 6175–6181.

14 R. G. Pearson, *J. Am. Chem. Soc.*, 1963, **85**, 3533–3539.

15 R. G. Pearson, *Inorg. Chem.*, 1988, **27**, 734–740.

16 K. Takao, S. Takao, Y. Ikeda, G. Bernhard and C. Hennig, *Dalton Trans.*, 2013, **42**, 13101–13111.

17 J. Narbutt, A. Wodyńska and M. Pecul, *Dalton Trans.*, 2015, **44**, 2657–2666.

18 L. Xu, Y. Hao, X. Yang, Z. Wang, C. Xu, N. E. Borisova, M. Sun, X. Zhang, L. Lei and C. Xiao, *Chem.-Eur. J.*, 2021, **27**, 10717–10730.

19 T. Kimura, M. Kaneko, M. Watanabe, S. Miyashita and S. Nakashima, *Dalton Trans.*, 2018, **47**, 14924–14931.

20 M. Kaneko and M. Watanabe, *J. Radioanal. Nucl. Chem.*, 2018, **316**, 1129–1137.

21 K. Takao, M. Kato, S. Takao, A. Nagasawa, G. Bernhard, C. Hennig and Y. Ikeda, *Inorg. Chem.*, 2010, **49**, 2349–2359.

22 T. Takeyama, S. Tsushima and K. Takao, *Inorg. Chem.*, 2021, **60**, 11435–11449.

23 H. Shi and Y. Yin, *Inorg. Chim. Acta*, 2014, **421**, 446–450.

24 T. P. DeAngelis and W. R. Heineman, *J. Chem. Educ.*, 1976, **53**, 594–597.

25 W. R. Heineman, *J. Chem. Educ.*, 1983, **60**, 305–308.

26 X. Q. Lin and K. M. Kadish, *Anal. Chem.*, 1985, **57**, 1498–1501.

27 A. Endo, I. Mochida, K. Shimizu and G. P. Sato, *Anal. Sci.*, 1995, **11**, 457–459.

28 G. M. Sheldrick, SHELXL Version 2018/3, *Acta Crystallogr., Sect. C: Struct. Chem.*, 2015, **71**, 3–8.

29 O. V. Dolomanov, L. J. Bourhis, R. J. Gildea, J. A. K. Howard and H. Puschmann, OLEX2: a complete structure solution, refinement and analysis program, *J. Appl. Crystallogr.*, 2009, **42**, 339–341.

30 A. Sabatini, A. Vacca and P. Gans, *Coord. Chem. Rev.*, 1992, **120**, 389–405.

31 M. J. Frisch, G. W. Trucks, H. B. Schlegel, G. E. Scuseria, M. A. Robb, J. R. Cheeseman, G. Scalmani, V. Barone, G. A. Petersson, H. Nakatsuji, X. Li, M. Caricato, A. V. Marenich, J. Bloino, B. G. Janesko, R. Gomperts, B. Mennucci, H. P. Hratchian, J. V. Ortiz, A. F. Izmaylov, J. L. Sonnenberg, D. Williams-Young, F. Ding, F. Lipparini, F. Egidi, J. Goings, B. Peng, A. Petrone, T. Henderson, D. Ranasinghe, V. G. Zakrzewski, J. Gao, N. Rega, G. Zheng, W. Liang, M. Hada, M. Ehara, K. Toyota, R. Fukuda, J. Hasegawa, M. Ishida, T. Nakajima, Y. Honda, O. Kitao, H. Nakai, T. Vreven, K. Throssell, J. A. Montgomery, J. E. Peralta Jr, F. Ogliaro, M. J. Bearpark, J. J. Heyd, E. N. Brothers, K. N. Kudin, V. N. Staroverov, T. A. Keith, R. Kobayashi, J. Normand, K. Raghavachari, A. P. Rendell, J. C. Burant, S. S. Iyengar, J. Tomasi, M. Cossi, J. M. Millam, M. Klene, C. Adamo, R. Cammi, J. W. Ochterski, R. L. Martin, K. Morokuma, O. Farkas, J. B. Foresman and D. J. Fox, *Gaussian 16, rev. C.01*, Gaussian, Inc., Wallingford, CT, 2016.

32 C. Lee, W. Yang and R. G. Parr, *Phys. Rev. B: Condens. Matter Phys.*, 1988, **37**, 785–789.

33 A. V. Marenich, C. J. Cramer and D. G. Truhlar, *J. Phys. Chem. B*, 2009, **113**, 6378–6396.

34 S. Grimme, J. Antony, S. Ehrlich and H. Krieg, *J. Chem. Phys.*, 2010, **132**, 154104.

35 A. Ikeda, C. Hennig, S. Tsushima, K. Takao and Y. Ikeda, *Inorg. Chem.*, 2007, **46**, 4212–4219.

36 K. Takao, S. Tsushima, T. Ogura, T. Tsubomura and Y. Ikeda, *Inorg. Chem.*, 2014, **53**, 5772–5780.

37 P. Macak, S. Tsushima, U. Wahlgren and I. Grenthe, *Dalton Trans.*, 2006, 3638–3646.

38 S. Tsushima, A. Rossberg, A. Ikeda, K. Muller and A. C. Scheinost, *Inorg. Chem.*, 2007, **46**, 10819–10826.

39 T. Takeyama, S. Iwatsuki, S. Tsushima and K. Takao, *Dalton Trans.*, 2022, **51**, 6576–6586.

40 E. D. Glendening, A. E. Reed, J. E. Carpenter and F. Weinhold, *NBO Version 3.1*.

41 R. Dennington, T. A. Keith and J. M. Millam, *Gauss View, ver. 6*, Semichem Inc., Shawnee Mission, KS, 2016.

42 S. S. Batsanov, *Inorg. Mater.*, 2001, **37**, 1031–1046.

43 U. Casellato, S. Sitran, S. Tamburini, P. A. Vigato and R. Graziani, *Inorg. Chim. Acta*, 1986, **114**, 111–117.

44 S. Sitran, D. Fregona, U. Casellato, P. A. Vigato, R. Graziani and G. Faraglia, *Inorg. Chim. Acta*, 1987, **132**, 279–288.

45 F. Zordan, L. Brammer and P. Sherwood, *J. Am. Chem. Soc.*, 2005, **127**, 5979–5989.

46 J. P. M. Lommers, A. J. Stone, R. Taylor and F. H. Allen, *J. Am. Chem. Soc.*, 1996, **118**, 3108–3116.

47 A. M. S. Riel, M. J. Jessop, D. A. Decato, C. J. Massena, V. R. Nascimento and O. B. Berryman, *Acta Crystallogr.*, 2017, **B73**, 203–209.

48 *Organic chemistry data*, ACS Division of Organic Chemistry, <https://organicchemistrydata.org/hansreich/resources/pka/>, (accessed August 2022).

49 R. S. Nicholson and I. Shain, *Anal. Chem.*, 1964, **36**, 706–723.

50 G. Nocton, P. Horeglad, V. Vetere, J. Pecaut, L. Dubois, P. Maldivi, N. M. Edelstein and M. Mazzanti, *J. Am. Chem. Soc.*, 2010, **132**, 495–508.

